Zhimin Liang, Xue Wang, Congwei Cai and Dianlong Wang*

Microstructure and Mechanical Properties of Thick Plate Friction Stir Welds for 6082-T6 Aluminum Alloy

Abstract: 6082-T6 aluminum alloy plate with thickness of 42 mm was butt welded by friction stir welding (FSW) from two sides. The microstructures of the joints exhibited different grain sizes because of unequal frictional heating and plastic flow during FSW process. The transition from the heat affected zone (HAZ) to the nugget zone (NZ) in thermos-mechanical affected zone of advancing side (AS-TMAZ) was more sudden than thermos-mechanical affected zone of retreating side (RS-TMAZ). Kissing bond (KB) defect throughout the entire FSW joint was displayed both at the grain boundary and in the interior of the grain with semi-continuous bands. KB had no direct effect on tensile properties. Vickers hardness of the FSW joint was lower than the BM because its high heat input, dissolved and coarsened precipitates and little to the grain size after FSW. Hardness distribution of double-sided welding joint showed X-shaped area softening characteristics, that is to say the lowest hardness was the junction of two welding joint of NZ and the junction of TMAZ and HAZ. The tensile fracture position occurred in the lowest hardness region of the FSW joint, and it did not occur in the KB defect position.

Keywords: 6082 aluminum alloy, friction stir welds (FSW), microstructure, mechanical properties, kissing bond (KB)

Introduction

The Al-Mg-Si alloys are commonly used for structural applications within the automotive, train and shipbuilding industry due to its excellent formability, good corrosion resistance and relative high mechanical properties. The 6082 aluminum alloy, as one type of these alloys, has been used in high-speed train manufacturing in China. When the conventional fusion welding methods were used to joint the alloy, a series of serious problems may appear including the formation of porosity, large welding deformation and high residual stresses [1]. Friction stir welding (FSW), which is a solid-state joining technique invented in 1991 by The Welding Institute (TWI), has many attractive advantages compared with the fusion welding processes, for example avoid of porosity, reduced deformation and decreased residual stresses [2].

The FSW joint is usually composed of four distinct zones, the base metal (BM), thermo-mechanical affected zone (TMAZ), the heat affected zone (HAZ), and the nugget zone (NZ). The BM is inevitably subject to additional thermal effects, but this is not enough to change its mechanical properties or microstructure. For heat-treatable aluminum alloys, the temperature needs to exceed 250℃ to treat the area as HAZ [3]. During the FSW, the NZ temperature can reach over 500℃. This zone showed a very fine grain structure [4]. However, for thick plate joint, the microstructure of NZ along the thickness direction is quite inhomogeneous [5]. It's important to study the organizational changes in its thickness. For 6XXX alloys, β' and β'' precipitations contribute mostly to strength and hardness improving [6]. The AS temperature is 5–10 K higher than the RS temperature [7].

Recently, the "kissing bond (KB)", or "lazy S" and "zigzag line" was generally found in the etched cross-section of FSW joint [8, 9]. Sato investigated that KB particles were Al_2O_3 oxide particles with an amorphous structure，which did not affect the root-bend property of the FSW joint [8]. When the FSW joint is not defective, the tensile strength of the joint is related to the hardness distribution. However, the tensile strength of FSW joint with KB defect inside the stir zone was much lower than that of the sound FSW joint [10]. The tensile fracture examination exposed a series of severe "scalloping" appearance in the joint with continuous KB flaw, while

*Corresponding author: Dianlong Wang, School of Materials Science and Engineering, Hebei University of Science and Technology, No. 26 Yuxiang Avenue, Yuhua District, Shijiazhuang 050018, China, E-mail: wdl@hebust.edu.cn
Zhimin Liang: E-mail: lianghebust@163.com, **Xue Wang:** E-mail: 785717539@qq.com, **Congwei Cai:** E-mail: caicongweiqi@163.com, School of Materials Science and Engineering, Hebei University of Science and Technology, No. 26 Yuxiang Avenue, Yuhua District, Shijiazhuang 050018, China

the sound FSW exhibited fine dimples [10]. Whether KB affected mechanical properties was required further study.

With the increase in the industrial application of aluminum alloy thick plates, especially in high-speed train, the comprehensive microstructure evolution and mechanical properties research are more significant. In this paper, we analyzed the microstructure and mechanical properties in friction stir double-sided butt welding of 6082-T6aluminum alloys with thickness of 42 mm by experimental investigation including microstructure examination, Vickers hardness and TEM. The experimental parameters and conclusions have practical significance for the actual production.

Materials and experimental procedures

Materials and welding method

The chemical composition of 6082-T6 aluminum alloy was shown in Table 1. The test specimens were couples of 42 mm × 150 mm × 500 mm. Prior to the welding, the oxide layer close to FSW groove was mechanically removed. The zero-gap butt joint configuration was obtained by special mechanical clamps. The FSW joint was double-side butt welded joint. The welding parameters were listed in Table 2. The welding tool was also shown in Figure 1.

Table 1: Chemical composition of the alloy (wt.%).

Si	Mg	Mn	Fe	Cu	Al
1.05	0.61	0.45	0.22	0.021	Bal.

Table 2: Welding parameters.

Spindle speed (R/min)	Travel speed (mm/min)	Friction pressure (KN)	Tool motion
400	110	1800	Anticlockwise

Microstructure and mechanical properties examination

Optical microscope was used to observe the microstructures in different zones on the top surface and the cross-
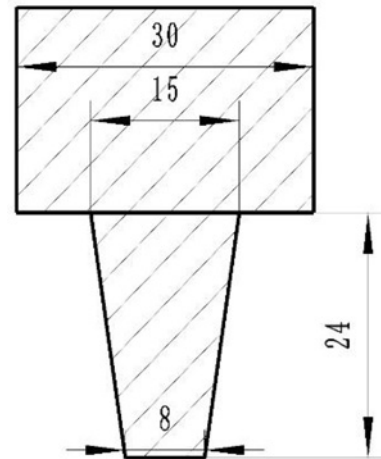

Figure 1: The diagram of welding tool (unit: mm).

section of the FSW joint. And the samples were etched using Keller's etch.

Transmission electron microscopy (TEM) was used to observe the precipitate particles in different zones of the FSW joint. The TEM thin foils specimens were mechanically milled to 50 μm thickness using abrasive papers and electropolished using 70 vol. % methanol and 30 vol. % nitric acid solution at −30℃ with a voltage of 10 V. And the specific sampling positions were shown in Figure 4 (with the indexed number from 1to 7).

Vickers hardness (HV) measurements were performed through the FSW joint of cross-section at different depths. The Vickers hardness was measured on a polished surface of the weld, using 500 g load and loading time were 10 s, respectively. The distance between the two neighboring test points was 1 mm to avoid possible interference of measurements. The locations of hardness points on the cross-section were shown in Figure 2.
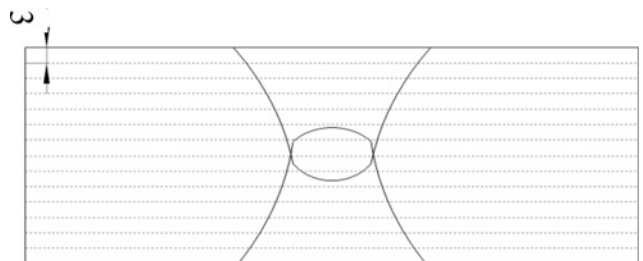

Figure 2: The locations of hardness testing points on the cross-section double-side FSW joint (unit: mm).

The tensile tests were carried out at room temperature using a Zwick Z600 electronic tensile testing machine. The dimensions of tensile test samples are shown in Figure 3. There were three samples for the tensile test.
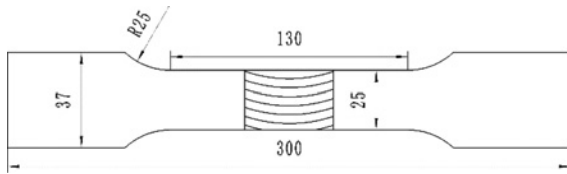
Figure 3: The dimensions of tensile test samples (unit: mm).

After testing, the fracture surfaces were examined using TESCAN-VEGAS scanning electron microscope (SEM).

Results and discussion

Microstructure observation

The macrostructure characterizations of the FSW joint were shown in Figure 4. The welded joint is divided into seven distinct regions along the cross-section including the shoulder-affected zone (SAZ), the middle of NZ, the bottom of NZ, thermomechanical affected zone of advancing side (AS-TMAZ), thermomechanical affected zone of retreating side (RS-TMAZ), the HAZ, and the base metal (BM), as shown in Figure 4(a). The macrostructure of the top surface of the FSW joint was shown in Figure 4(b). Figure 5 showed the microstructures of the cross-section and top of TMAZ in the FSW joint. The transition from the HAZ to NZ was more sudden on the AS-TMAZ (see Figure 5a, c) than the RS-TMAZ (see Figure 5b, c). It can be explained on the basis of the flow and thermal behavior of material model developed by Hamilton et al [6]. A sharp boundary develops on the AS-TMAZ as the rising flow from the work piece bottom and the downward flow from the work piece surface oppose one to another with very little cross flow [6]. And the model suggests that RS-TMAZ is strong material
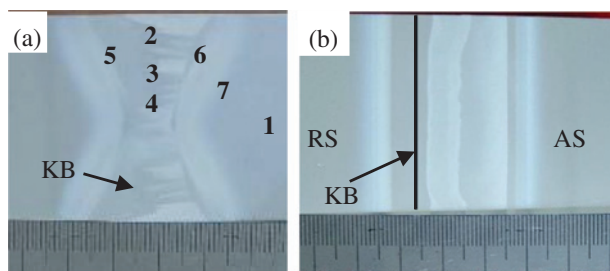

Figure 4: Macrostructure of the FSW joint: (a) cross-section: (1) BM (2) SAZ (3) Middle of NZ (4) Bottom of NZ (5) RS-TMAZ (6) AS-TMAZ (7) HAZ; (b) Top Surface: KB (kissing bond).
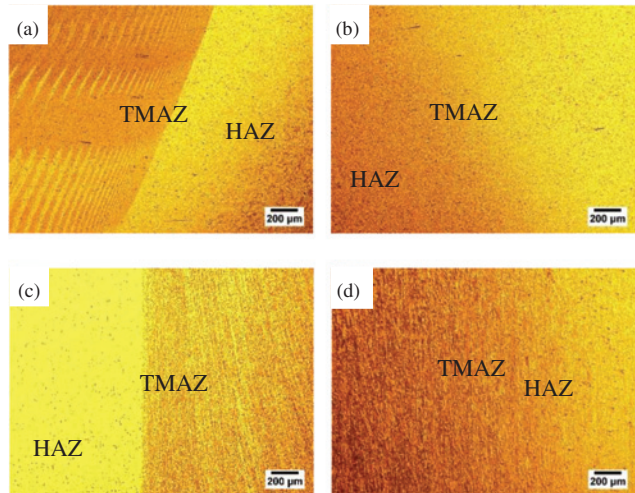

Figure 5: Microstructures of the TMAZ. (a) Cross-section of AS-TMAZ; (b) Cross-section of RS-TMAZ; (c) Top surface of AS-TMAZ; (d) Top surface of RS-TMAZ.

flow cross the boundary, so the RS-TMAZ boundary is diffused and gradual [11]. And there is a noticeable stir pattern on the advancing side in cross-section. Figure 6 showed microstructure of grain size distribution in the transverse cross–section of the FSW joint. This can be attributed to the degree of heat input and the concomitant grain growth [12]. Slightly coarser grains were observed in the BM (Gave = 7.24 μm) (see Figure 6a). Comparing the grain sizes of the SAZ (Gave = 5.37 μm), middle of NZ (G_{ave} = 5.84 μm) and bottom of NZ (Gave = 2.51 μm), the bottom of NZ exhibited refined grains, most likely due to the impact of double stirring of the tool needle (see Figure 6b, c, d). The grain size of HAZ (Gave = 5.84 μm) was slightly coarser than that of AS-TMAZ (Gave = 3.50 μm) and was similar to that of RS-TMAZ (Gave = 5.78 μm) (see Figure 6e, f, g). The grain size on the RS-TMAZ was coarser than that on the AS-TMAZ. This was related to the flow and thermal behavior of material mentioned earlier.

The zigzag line was the presence of oxide particles, which formed semi-continuous bands from the SAZ to the bottom of the NZ, known as KB. Overview image of KB was shown in Figure 4(a). The model of the KB was shown in Figure 7. The KB ran through the entire weld. Top surface of the FSW joint was the XY surface (see Figure 7), and KB was shown in Figure 8(a). Figure 8(b) showed the detail of KB with a zig-zag shape. The cross-section surface of the FSW joint was the XZ surface (see Figure 7). KB of the cross-section was shown in Figure 9. The width of the KB was not uniform. The KB in the cross-section changed complex and diverse. The complex change of the KB was closely related
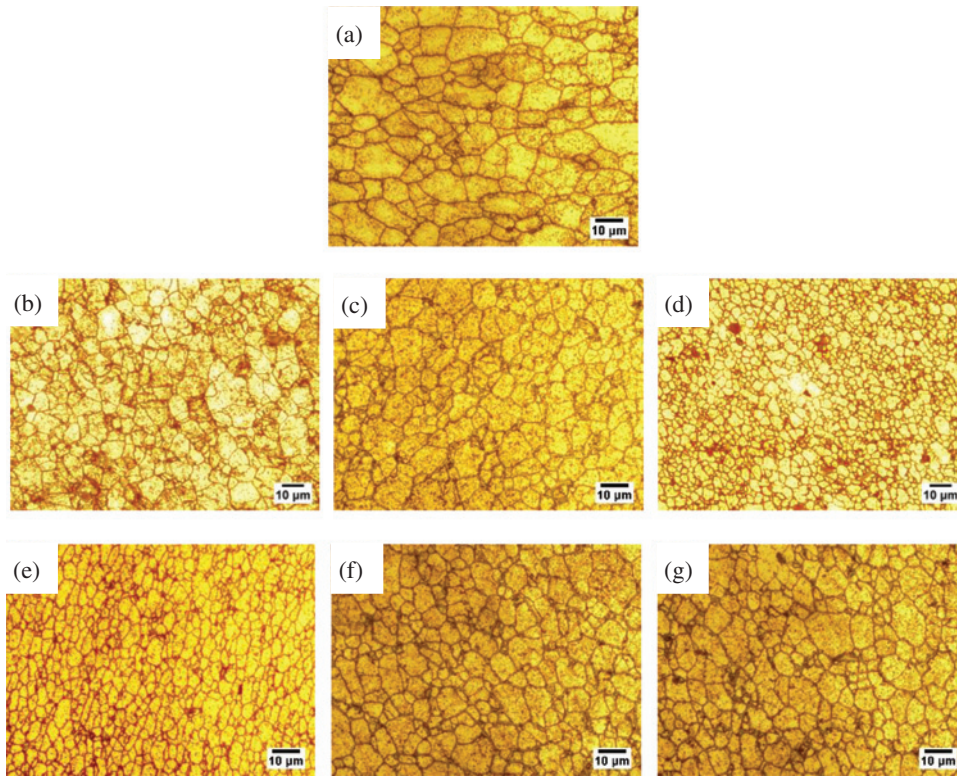
Figure 6: Microstructures of grain size distribution in the cross –section of the specimen: (a) BM (G_{ave} = 7.24 μm); (b) SAZ (G_{ave} = 5.37 μm); (c) Middle of NZ (G_{ave} = 5.84 μm); (d) Bottom of NZ (G_{ave} = 2.51 μm); (e) AS-TMAZ (G_{ave} = 3.50 μm); (f) RS-TMAZ (G_{ave} = 5.78 μm); (g) HAZ (G_{ave} = 5.84 μm).

Figure 7: The model of the KB (kissing bond) line in space.
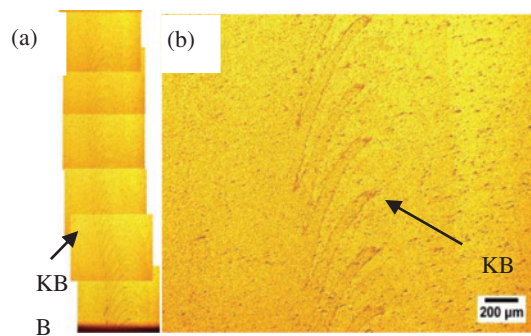

Figure 8: Kissing bond (KB) of XY surface of FSW joint. (a) Overview of kissing bond (KB); (b) Detail of kissing bond (KB).

to plastic flow. Figure 10 showed the relationship between the position of KB and grain. Figure 10(a) showed the microstructure of a thinner position of KB line Figure 10(b) showed the microstructure of a thicker position of KB line. It can be seen that the KB exist both at the grain boundary and in the interior of the grain with semi-continuous bands.

TEM analysis

The locations of TEM thin foils were shown in Figure 4(a) (1 to 7 is the location of the TEM thin foils). Figure 11 presented TEM results obtained from the FSW joint. The BM contains high-density of needle-shaped precipitates β″ (average thickness is 3 nm) which were contributes to the hardness of the material (see Figure 11a). The precipitates β were often formed above 300°C [13]. The precipitates β was relatively coarsen and the enhancement effect was usually poor [13]. Comparing the thickness precipitates β of SAZ, middle of NZ and bottom of NZ, the precipitates β of bottom of NZ (average thickness is 16 nm) were slightly coarser than that of middle of NZ
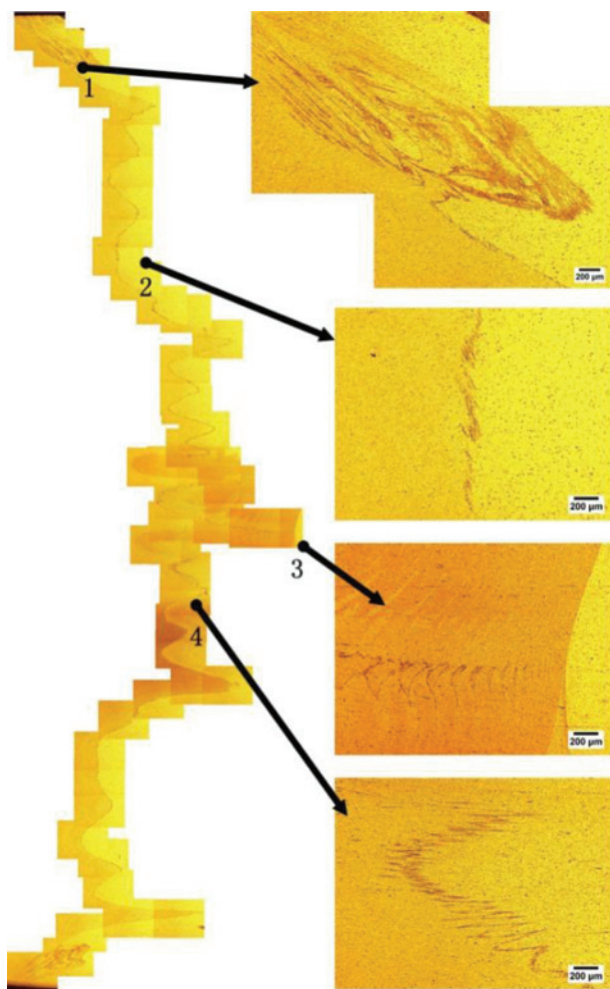
Figure 9: Kissing bond (KB) of XZ surface of FSW joint.

Figure 10: The relationship between the position of Kissing bond (KB) and grains. (a) Thinner position of KB line; (b) Thicker position of KB line.

(average thickness is 12 nm) and SAZ(average thickness is 10 nm) (see Figure 11b, c, d). The precipitates were also dissolved in FSW joints compared with BM. The AS-TMAZ had a grain structure with a relatively high density of dislocation pile-up (see Figure 11e). The sub-boundaries were observed in the grain boundary in RS-TMAZ (see Figure 11f).

Vickers hardness

The Vickers hardness measured across the FSW joint was shown in Figure 12. Hardness distribution of double-sided welding joint showed X-shaped area softening characteristics. The difference in hardness was observed in FSW joint. The lowest hardness was the junction of two bead of NZ and the junction of TMAZ and HAZ (ranged from 48 to 70 HV). The hardness along the weld thickness direction in the SAZ, the middle of NZ
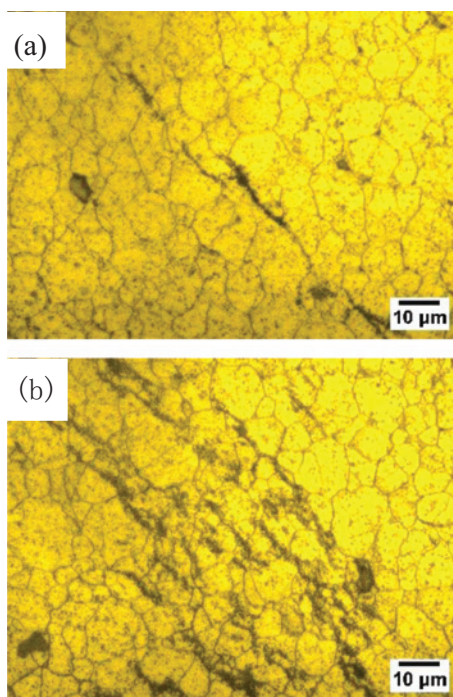
and the bottom of NZ, appeared lower than previous ones. The hardness increased from the HAZ to the BM (ranged from 100 to 115 HV). For the 6XXX alloys, precipitate hardening is the main strengthening mechanism and the strength can be measured by hardness test. The FSW process tends to soften the alloys because of the high heat input dissolved and coarsened precipitates [14]. Sato Studied the relationship between hardness and precipitation distribution in AA6063-T5, taking into account the effect of grain size during the FSW [15]. The results showed that the hardness was mainly affected by precipitation hardening, and little effect to the grain size after FSW. Figures 6 and 12 showed that the grain size of the bottom of NZ was refine, but the hardness was low. The precipitates β of the bottom of NZ were slightly coarser than that in the middle of NZ and SAZ. That was to say, the grain size had little effect on the hardness of the FSW. The main factor affecting hardness was the precipitates.

Tensile test

Macroscopic fractured surfaces of the FSW joint after tensile tests were shown in Figure 13. Typical mechanical properties of FSW joint were listed in Table 3. The

Table 3: Tensile tests.

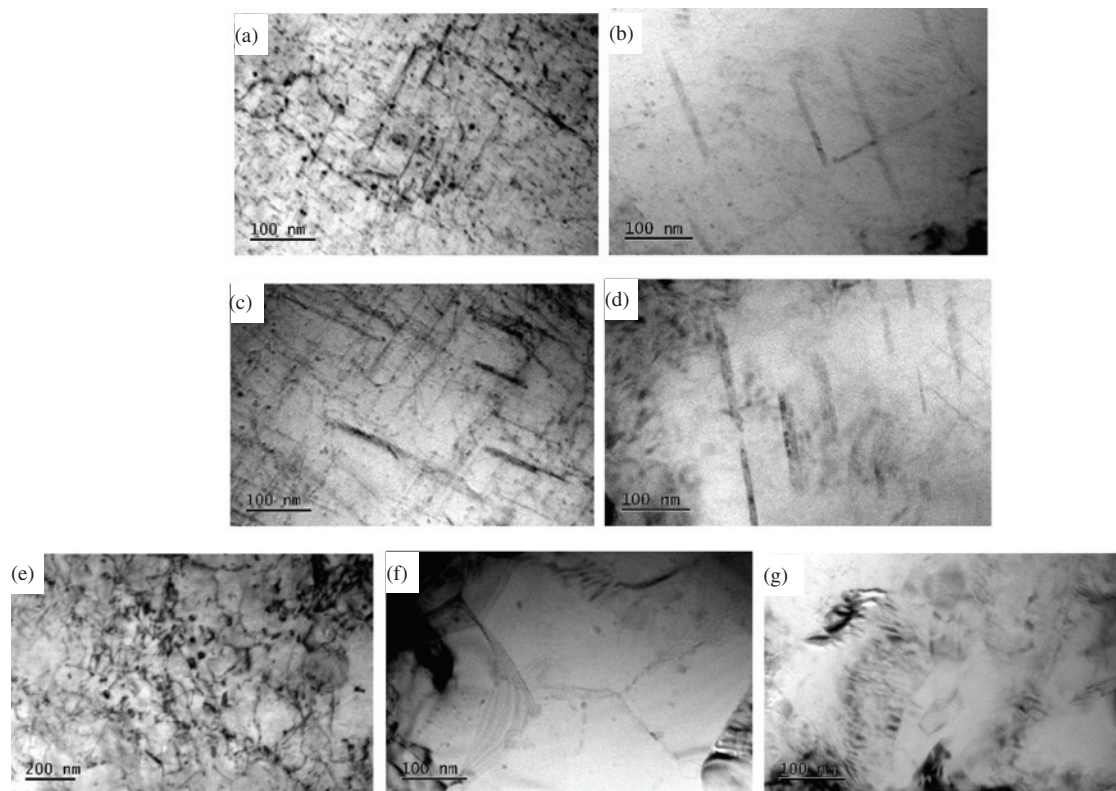| Tensile data	Ultimate tensile strength (MPa)	0.2% yield strength (MPa)	Percent elongation at fracture (%)
1	224.9	145.8	6.1
2	226.3	146.2	5.9
3	225.7	144.9	6.1
Average	225.6	145.6	6.0

average tensile strength was 225.6 MPa and the average elongation was 6%. Failure occurred in the FSW joint for two types of samples. The FSW joint exhibited a ductile shear fracture in the sample 1、2、3 fracture with a shear angle of 45° in the HAZ near the TMAZ. The tensile fracture position occurred in the lowest hardness region of the FSW joint. It did not occur in the KB position. KB line had no direct effect on the location of the fracture. Figures 14 and 15 showed the SEM images of the test fracture surface of the sample 1, 2 of FSW joint. The dimples of the fractured surface indicated that the fracture was the ductile fracture. However, there were also brittle fracture characteristics in the fracture surface in Figures 14(e) and 15(d).

Conclusions

The mechanical and metallurgical behavior of 6082-T6 aluminum alloy was studied in this paper. The microstructures exhibited different grain sizes because of the frictional heating and the plastic flow during FSW process. Slightly coarser grains were observed in the BM. The grain size of HAZ was slightly coarser than that of AS-TMAZ but similar to that of RS-TMAZ. The transition from the HAZ to NZ was more sudden on the AS-TMAZ than the RS-TMAZ; FSW joint had KB defect. The KB ran through the entire weld. It can be seen that the KB exist both at the grain boundary and in the interior of the grain with semi-continuous bands. KB had no direct effect on tensile properties.

TEM showed that high density of needle-shaped precipitates β″ were observed in the BM. β″ precipitations contribute BM hardness improving. The precipitates β of bottom of NZ were slightly coarser than that of middle of NZ and SAZ. Coarse precipitates β enhancement effect was poor.

The Vickers hardness of the welded zones was lower than the BM because of the high heat input dissolved and coarsened the precipitates. The lowest hardness was the

Figure 11: Precipitate particles in the interior grain of: (a) BM; (b) SAM; (c) Middle of NZ; (d) Bottom of NZ; (e) AS-TMAZ; (f) RS-TMAZ; (g) HAZ.
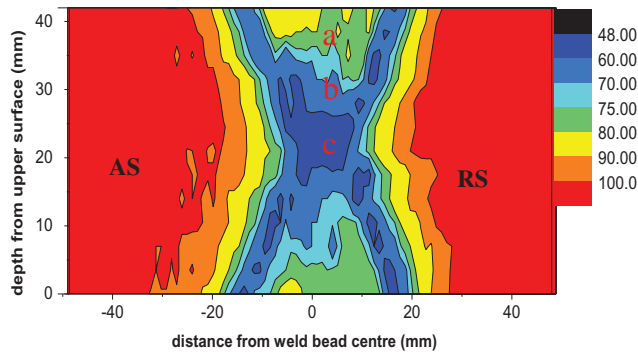
Figure 12: Map of Vickers hardness of FSW joint. Note: (a) SAZ; (b) Middle of NZ; (c) Bottom of NZ.
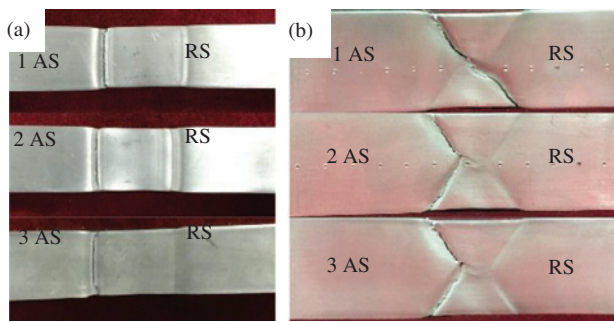

Figure 13: Macroscopic observations for fractured surfaces of the FSW joint.

junction of two welding joint of NZ and the junction of TMAZ and HAZ.

According to the microstructure and Vickers hardness experiments, we conclude the relationship between microstructure and hardness. The grain size of the bottom of NZ (Gave = 2.51 μm) was refine, but

the hardness was the lowest. Slightly coarser grains were observed in the BM (Gave = 7.24 μm), but the hardness was the highest in the joint. That was to say, grain refinement did not determine the hardness of the material. The main factor affecting hardness was the precipitates. Precipitations β″ (average thickness is 3 nm) contribute BM hardness (ranged from 100 to 115 HV) improving. The precipitates β of bottom of NZ (average thickness is 16 nm) were slightly coarser than that of middle of NZ (average thickness is 12 nm) and SAZ (average thickness is 10 nm). The hardness of bottom of NZ (ranged from 48 to 60 HV) was lower than middle of NZ (ranged from 60 to 75 HV) and the SAZ (ranged from 75 to 80 HV). Coarse precipitates β enhancement were poor and regarded as unfavorable precipitates, due to the severe reduction in hardness. The precipitates β″ dissolution of HAZ and TMAZ caused the lower hardness. So the reduction in the hardness of the FSW joint was associated with high heat input dissolved and coarsened the precipitates.

The test samples average ultimate tensile strength was 225.6 MPa and the average elongation was 6%. The FSW joint exhibited a ductile shear fracture in the samples fracture surface with a shear angle of 45° in the HAZ near the TMAZ. The tensile fracture position occurred in the minimum hardness region of the FSW joint. And it did not occur in the KB position.
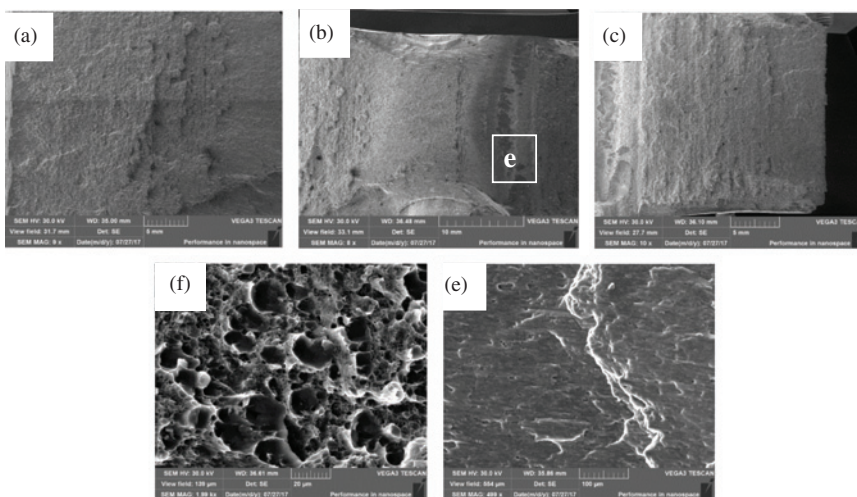
Figure 14: SEM images of test fracture surface of the sample 1. (a) Top surface area; (b) Centre area; (c) Bottom surface area.
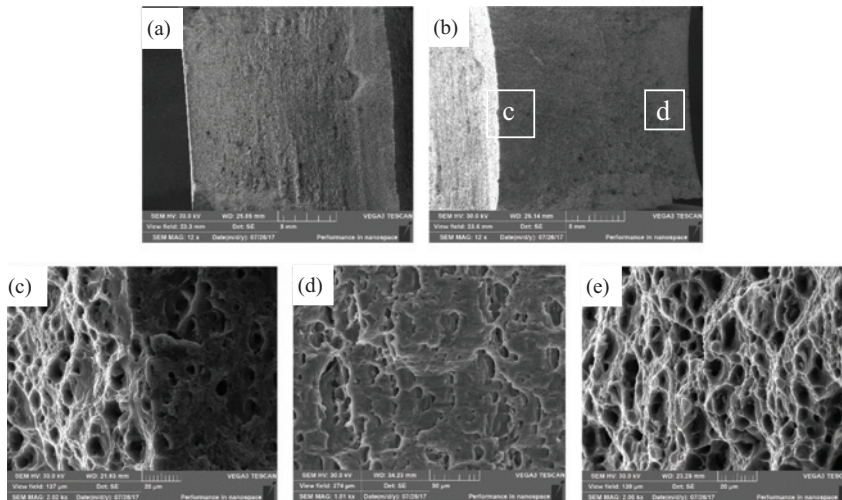
Figure 15: SEM images of test fracture surface of the specimen 2: (a) Top surface area; (b) Centre and bottom surface area.

References

[1] B.T. Gibson, D.H. Lammlein, T.J. Prater, W.R. Longhurst, C.D. Cox, M.C. Ballun, K.J. Dharmaraj, G.E. Cook and A.M. Strauss, J. Manuf. Process., 16 (2014) 56–73.

[2] S.B. Dunkerton, D.E. Nicholas and P.D. Sketchley, Great Britain Patent Application No. 9125978, 1991.

[3] M.W. Mahoney, C.G. Rhodes, J.G. Flintoff, R.A. Spurling and W.H. Bingel, Metall. Mater. Trans. A., 29 (1998) 1955–1964.

[4] W.D. Lockwood, B. Tomaz and A.P. Reynolds, Mater. Sci. Tech-Lond., 323 (2002) 348–353.

[5] N. Guo, Y.L. Fu, Y.Z. Wang, Q. Meng and Y.X. Zhu, Mater. Des., 113 (2017) 273–283.

[6] I.J. Polmear, Light Alloys: Metallurgy of the Light Metals, Haistead Press (1996), pp. 39–40.

[7] C. Hamiton, M. Kopyściański, O. Senkov and S. Dymek, Metall. Mater. Trans. A., 4 (2013) 1730–1740.

[8] Y.S. Sato, F. Yamashita, Y. Sugiura, S.H.C. Park and H. Kokawa, Scripta Mater., 50 (2004) 365–369.

[9] C. Zhou, X. Yang and G. Luan, J. Mate. Sci., 41 (2006) 2771–2777.

[10] H.B. Chen, J.F. Wang, G.D. Zhen, S.B. Chen and T. Lin, Mater. Des., 86 (2015) 49–54.

[11] C. Ravi and C. Wolverton, Acta. Mater., 52 (2004) 4213–4227.

[12] S.A. Askariani, H. Pishbin and M.M. Javadi, J. Alloy Compd., 724 (2017) 859–868.

[13] M. Esmaily, N. Mortazavi, W. Osikowicz, H. Hindsefelt, J.E. Svensson, M. Halvarsson, G.E. Thompson and L.G. Johansson, Corros. Sci., 111 (2016) 98–109.

[14] Y.S. Sato, H. Seung, C. Park and H. Kokawa, Metall. Mater. Trans. A., 32 (2001) 3033–3042.

[15] Y.S. Sato, H. Kokawa, M. Enomot and S. Jogan, Metall. Mater. Trans. A., 30 (1999) 3125–3130.